Barrier Properties of Polypropylene/Organoclay Nanocomposites

M.-J. Dumont,[1] A. Reyna-Valencia,[1] J.-P. Emond,[2] M. Bousmina[1]

[1]*Department of Chemical Engineering, Laval University, Ste-Foy, QC, G1K 7P4 Canada*
[2]*Department of Food Engineering, Laval University, Ste-Foy, QC, G1K 7P4 Canada*

Received 14 August 2005; accepted 2 July 2006
DOI 10.1002/app.25253
Published online in Wiley InterScience (www.interscience.wiley.com).

ABSTRACT: Polypropylene/clay nanocomposites are attractive candidates for applications requiring good barrier properties because of the inherent features of the polymer matrix. To assess their potential, systematic research relating the barrier performance to the structural characteristics of polypropylene/montmorillonite samples has been conducted. The nanocomposites have been tested in the presence of helium, water vapor, toluene, and methanol, and the unmodified matrix has been found to exhibit better properties than its mixtures with the compatibilizer and/or clay. The method for the interpretation of the results proposed in this study considers the composition of the samples, the morphology of the semicrystalline polymer matrix, and the state of dispersion/exfoliation of the clay layers, along with the specific interactions between the solvent molecules and the system components. In this way, several points have been identified for understanding and improving the performance of the nanocomposites. © 2006 Wiley Periodicals, Inc. J Appl Polym Sci 103: 618–625, 2007

Key words: barrier; nanocomposites; poly(propylene) (PP)

INTRODUCTION

Polymers are broadly used in ubiquitous applications that demand good barrier properties, such as food packaging and automotive gasoline containers. The long list of common barrier polymers includes polypropylene (PP) and ethylene vinyl alcohol (EVOH) copolymers. No single polymer, however, has shown the ideal combination of performance features. For instance, PP possesses good water-vapor barrier properties, but it is easily permeated by oxygen, carbon dioxide, and hydrocarbons. In contrast, EVOH offers excellent resistance to oxygen, carbon dioxide, and hydrocarbons but rapidly loses its properties when exposed to moisture.[1] The necessity of developing more effective barrier polymers has given rise to different strategies to incorporate and optimize the features from several components. The aim is to come up with materials that have low permeability to specific gases and vapors, high solvent resistance, good mechanical stability, and low cost as inherent characteristics.

Correspondence to: M. Bousmina (bousmina@gch.ulaval.ca).

Contract grant sponsor: Natural Sciences and Engineering Research Council of Canada.
Contract grant sponsor: Canada Research Chair on Polymer Physics and Nanomaterials.
Contract grant sponsor: Steacie Fellowship Grants.

Coextrusion is used to generate multilayer structures in which various polymers are sandwiched together. The resulting films comprise at least five layers, such as the PP/adhesive/EVOH/adhesive/PP system: an EVOH barrier sheet trapped between two layers of moisture-resistant PP and two additional adhesive strata (e.g., anhydride-grafted PP) to keep the array together.[1] Coextrusion is a complex and expensive process, and polymer blending has been proposed as an alternative. Successful barrier films made of PP/EVOH blends essentially require an oriented lamellar morphology of EVOH dispersed in a PP matrix, which is obtained only with special extrusion dies and proper copolymers.[2]

Recent developments in polymer nanocomposites have attracted attention to the possibilities offered by this technology to enhance the barrier properties of inexpensive resins. To date, several studies have demonstrated improvements in permeability reduction to gases, moisture, and organic vapors resulting from the addition of low concentrations of layered-clay nanoparticles to various thermoplastic matrices. There is the case of a 40% drop in oxygen permeability upon the incorporation of 4 vol % organomontmorillonite (OMMT) into high-density polyethylene, as reported by Osman et al.[3] Similarly, Yano et al.[4] obtained a 10-fold reduction in the water vapor permeability coefficient of a polyimide containing 2 wt % mica nanoparticles in comparison with the unfilled polymer. The improved nanocomposite barrier behavior illustrated by these examples has

been explained by the tortuous path model, in which the presence of impermeable clay platelets generates an overlapped structure that hinders penetrant diffusion and thus decreases the permeability of the material.[5] The permeability of a nanocomposite system normally depends on the clay content, length-to-width ratio, relative orientation, and degree of dispersion (intercalated, exfoliated, or intermediate state) of the silicate layers.[6] In particular, a high length-to-width or aspect ratio of the clay lamellae is a key factor in maximizing tortuosity.

PP/clay nanocomposites can be prepared through the melt blending of the bulk polymer with modified clay and with functionalized oligomers [maleic anhydride grafted propylene (PP-*g*-MA)] as compatibilizers.[7,8] The structural characterization of PP/organoclay hybrids has yielded relevant information about the influence of the composition (i.e., clay and compatibilizer contents) and the processing conditions on the morphological features that determine the barrier properties, such as the degree of intercalation of the polymer chains in the silicate galleries, the extent of exfoliation of clay lamellae, and the generated crystalline structures.[9–12] Recent studies on the transport properties of PP/organoclay nanocomposites for various organic vapors have reported a permeability decrease in dichloromethane and *n*-pentane in comparison with unmodified PP.[13,14] The diffusion coefficient decreases with increasing silicate content (synthetic fluorohectorite modified with protonated octadecylamine), showing that the enhancement in the barrier properties of these systems can be obtained by control over their composition.

This work focuses on the permeability of PP/OMMT nanocomposites to gases (helium), moisture, and organic vapors (methanol and toluene) to assess their barrier properties in a range of conditions and prescreen their potential for practical applications. The results from the barrier-property tests have been related to the composition and the morphological characteristics of the samples, which have been investigated with wide-angle X-ray diffraction (WAXD) and transmission electron microscopy (TEM). Furthermore, the effects of the specific interactions between the penetrant molecules, the polymer chains, and the virgin and organically modified clay surfaces are taken into account in the discussion.

EXPERIMENTAL

Materials

The materials employed in this study were a PP homopolymer (grade PDC1274, Basell Polyolefines, Varennes, Canada), natural montmorillonite organically modified with a quaternary ammonium salt (OMMT; Cloisite 20A, Southern Clay Products, Gonzales, TX), and PP-*g*-MA [1.2 wt % maleic anhydride (MA); Polybond 3000, Crompton Corporation, Middlebury, CT] as a compatibilizer. Clay particles were used as received, without washing or any additional modifications.

TABLE I
Compositions of the Testing Samples

Sample	PP (wt %)	PP-*g*-MA (wt %)	OMMT (wt %)
PP	100	0	0
97/0/3	97	0	3
94/0/6	94	0	6
94/3/3	94	3	3
88/6/6	88	6	6
82/18/0	82	18	0
80/10/10	80	10	10
76/18/6	76	18	6
Clay	0	0	100

Sample preparation

Nanocomposites with different proportions of the clay and compatibilizer were prepared via melt blending in a ThermoHaake PolyLab Rheomix batch mixer (Thermo Electron Corporation, Waltham, MA) under the following conditions: a processing temperature of 180°C, a mixing time of 10 min, and a rotor speed equal to 60 rpm. Table I summarizes the compositions of the samples used to investigate the effects of the clay content and compatibilizer concentration on the barrier properties; virgin PP was the reference material.

The sheets for the barrier-performance tests as well as the samples for the structural studies (WAXD and TEM) were formed via compression molding in a Carver laboratory press (Carver, Inc., Wabash, IN) at 200°C. Cold water was used to bring the platens to room temperature while full holding pressure was maintained. The average thickness of the samples was 1.52 mm for the sheets, 0.81 mm for the moisture-barrier test samples, and 1.55 mm for the rectangular WAXD specimens. The TEM specimens (50–70 nm thick) were prepared by ultramicrotomy from sections of the molded samples cryogenically reduced to powder and embedded in an epoxy resin. The crystallization conditions from the molten state were not controlled in this study (see the Results and Discussion section for further details).

Methods of characterization

An overview of the crystalline structure of the samples was obtained by WAXD. The dispersion of clay layers within the PP matrix was analyzed by WAXD and TEM. WAXD measurements were performed with a Siemens/Bruker diffractometer (Bruker AXS, Inc., Madison, WI) with copper radiation and a

graphite monochromator. TEM images were obtained via a JEOL JEM-1230 (JEOL USA, Inc., Peabody, MA) apparatus with an acceleration voltage of 30 kV.

The helium barrier properties of the nanocomposite materials were assessed with an Alcatel model ASM142 helium leak detector (Alcatel Vacuum Technology, Hingham, MA) at 23°C. In the test cell, the polymeric sheet under investigation was subjected to a pressure differential: the high-pressure side was exposed to a helium feed at a constant pressure (in this case, nearly 0.7 atm), whereas the low-pressure side was kept *in vacuo* for trapping the permeating gas molecules. A detector was connected to the vacuum chamber of the cell. In the steady state, the leak was independent of the volume (area and thickness) of the sheet and of the upstream pressure of the cell. The gas flow (mbar L/s) was calculated by the multiplication of the volume of helium passing through the sheet per unit of time by the downstream pressure in the circuit.

The water-vapor transmission rate (WVTR; g/m^2 day) was measured with a Permatran-W 3/31 system from Mocon, Inc. (Minneapolis, MN), in which the polymer sheet dividing the test cell into two halves was exposed to water vapor flowing in the upper half. A carrier gas collected the permeating molecules in the lower half of the cell and took them to a sensor. Tests were performed at 100% relative humidity and 23°C.

The transmission rate tests of methanol and toluene vapors were carried out at 40°C with a home-developed technique that can be summarized as follows. The nanocomposite sheet was placed horizontally between two cylindrical aluminum reservoirs; the lower container enclosed the testing hydrocarbon, and the upper container was connected to a sampling device. The test cell was sealed and placed in an environmental chamber under a controlled temperature. The permeating vapors were collected automatically by means of a carrier gas at different time intervals and stored in small tubes containing activated carbon as an absorbent for retaining the vapor molecules. When the test time was over, the analytes were desorbed automatically with a TurboMatrix system (PerkinElmer, Wellesley, MA) and quantified directly via an HP 5890 series II gas chromatograph (Hewlett Packard, Mississauga, Canada). The results are expressed as g/m^2 day.

The molecular interactions between the virgin and organically modified silicate layers and the organic solvents (i.e., methanol and toluene) were investigated by IR spectroscopy with an ABB Bomem spectroscope (ABB Inc., Norwalk, CT). The clay particles were immersed in the solvent and analyzed in a cell between two windows of CaF_2. For comparison, clay alone and the pure solvents were also studied with this technique.

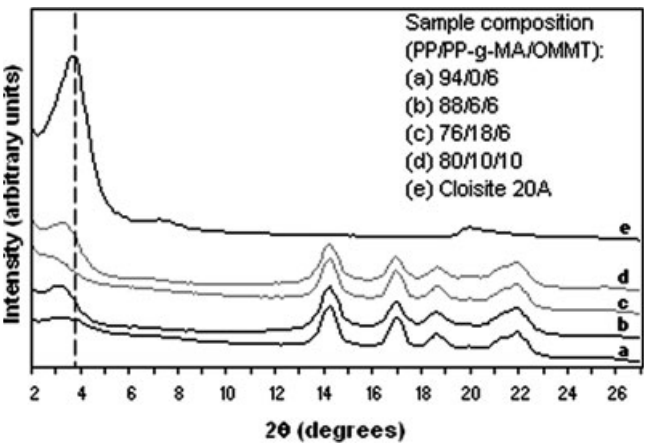

Figure 1 WAXD curves of montmorillonite and PP/PP-*g*-MA/OMMT samples prepared with different compositions. The traces have been vertically displaced for clarity.

RESULTS AND DISCUSSION

State of the semicrystalline structure

Overall, the crystallization process of the nanocomposite sheets occurred under nonisothermal conditions upon cooling from the molten state at various cooling rates (faster in the initial stage and slower when room temperature was approached). The WAXD curves obtained for four different semicrystalline PP/PP-*g*-MA/OMMT nanocomposites are shown in Figure 1. The peaks of the diffracted intensities, which are distinctive of the crystalline domains, are located at the same values of 2θ in traces a–d, 14.2, 17.0, 18.7, and 21.3°, which correspond to the (110), (040), (130), and (111) planes of the monoclinic α structure of PP, respectively.[15] At first sight, these results suggest that the crystalline fraction and morphology of the nanocomposite samples with different compositions remain practically the same, but it should be taken into account that the amounts of the filler and compatibilizer can modify certain structural parameters. Usually, the presence of inorganic filler particles affects the nucleation and spherulite growth steps in the crystallization process of the PP matrix, depending on the interactions at the interface.[16] Maiti et al.[10] observed that clay particles increase the nucleus density and generate smaller spherulites in isothermally crystallized PP-*g*-MA/OMMT systems in comparison with the unfilled matrix. Moreover, functional groups grafted onto the PP backbone lead to a decrease in the perfectibility of the spherulites.[17]

In this particular case, the state of the crystalline domains can be deduced from the preparation conditions (composition and processing) of the nanocomposite samples. During rapid cooling, nuclei form as the temperature decreases, but spherulite growth is limited by kinetic criteria. Therefore, the structure that develops is that with the maximum

growth rate, characterized by small crystallites exhibiting a very low degree of perfection, which act as crosslinks between highly disordered amorphous regions.[15] Under these circumstances, it can be assumed that the high cooling rates minimize the possible structural differences arising from the presence of various amounts of the filler and compatibilizer in the nanocomposite samples.

In the discussion that follows about barrier properties, the permeability of the various samples to the diffusing molecules is assumed to be unaffected by the state of the crystalline domains because the semicrystalline structure is thought to be fairly similar for all samples. Moreover, the influence of crystallization on the intercalation of clay particles in the PP matrix observed by Maiti et al.[10] can be neglected in this study because of the processing conditions detailed previously; indeed, the conditions required for intercalation to occur during crystallization are high temperatures and long crystallization times.[10]

State of the nanoparticles in the polymer matrix

The state of intercalation of clay stacks in the nanocomposites can be assessed from WAXD data. The characteristic peak of clay corresponding to the (001) plane of the silicate layers is located at $2\theta = 3.7$ in trace e of Figure 1. The patterns generated by composites prepared with a constant concentration of the filler and variable amounts of the compatibilizer (traces a–c), as well as a higher weight percentage of nanoparticles (trace d), show a small peak or shoulder in the same region of 2θ but slightly shifted to the left. For the sample prepared without the compatibilizer, the peak is very broad and ill defined. In contrast, upon the addition of PP-*g*-MA, the peak is clearly resolved for the system with 6 wt % compatibilizer, becoming a shoulder when 18 wt % PP-*g*-MA is used. When the amount of clay is increased to 10 wt %, reducing the concentration of the compatibilizer, the peak appears again. Peaks in traces b and d indicate that there is a significant fraction of clay layers arranged in intercalated stacks (see the interpretation of TEM images for complementary information), whereas the shoulder in trace c indicates that the ordered structures have been modified to some extent. Lattice distortions are likely to cause the peak broadening in trace a, suggesting that significant fractions of amorphous polymer chains surround the regular clay stacks instead of penetrating the interlamellar galleries because of the lack of affinity between OMMT and PP molecules.

The spacing between clay layers can be calculated from the location of the intensity peaks with Bragg's well-known diffraction law, $d = \lambda/2 \sin \theta$, where d is the interlamellar distance, λ is the wavelength of the X-ray (1.54 Å), and θ is the diffraction angle. As expected, the results presented in Table II indicate that the addition of the compatibilizer increases gradually the interlayer spacing as a result of the intercalation of polymer molecules. The broad shoulder that corresponds to the system with the highest amount of compatibilizer provides an approximate result that evidences the greatest interlayer distance and suggests that the clay stacks have lost their regularity, probably because of the relative and partial exfoliation. The increase in the clay content at the expense of the concentration of the compatibilizer hinders the intercalation–exfoliation process and maintains the regular ordering of the clay stacks.

TABLE II
Clay Interlayer Spacing (*d*-Spacing) in PP/OMMT Nanocomposites

Sample composition (wt %)[a]	Peak location in the 2θ scale (°)[b]	*d*-spacing (nm)
Clay	3.7	2.39
88/6/6	3.2	2.76
76/18/6	$\approx$ 2.6	3.39
80/10/10	3.3	2.67

[a] PP/PP-*g*-MA/OMMT.
[b] From X-ray analysis.

Complementary information on the morphology of the nanocomposites was obtained with TEM. The images shown in Figure 2 illustrate the effects of the composition on the development of the nanostructure. In the sample prepared without the compatibilizer [Fig. 2(a)], the clay particles were agglutinated, and this proved that the driving force for intercalation was not strong enough. In contrast, the system prepared with 18 wt % compatibilizer was partially exfoliated [Fig. 2(b)]. Figure 2(c,d) compares two specimens that exhibit a heterogeneous, intercalated–exfoliated structure formed by both stacks and individual platelets. The specimen in Figure 2(c) shows a better dispersion of the silicate layers because the clay content was lower. In both cases, it can be concluded that a higher concentration of the compatibilizer would be required to improve the intercalation and exfoliation of the filler stacks. The average length of the clay layers estimated from these images is about 113 nm, and this means that the processing conditions do not cause platelet attrition.

The morphology developed in sample 76/18/6 is close to the desired delaminated structure and becomes the focus of further attention. Generally, particle exfoliation has been explained by the specific interactions between the polar MA groups of the compatibilizer and the organically modified surface of the clay layers. In addition, OH groups present in the unmodified side areas of clay might be able to react with MA according to the mechanism proposed in Figure 3. The partially negative hydroxyl groups of

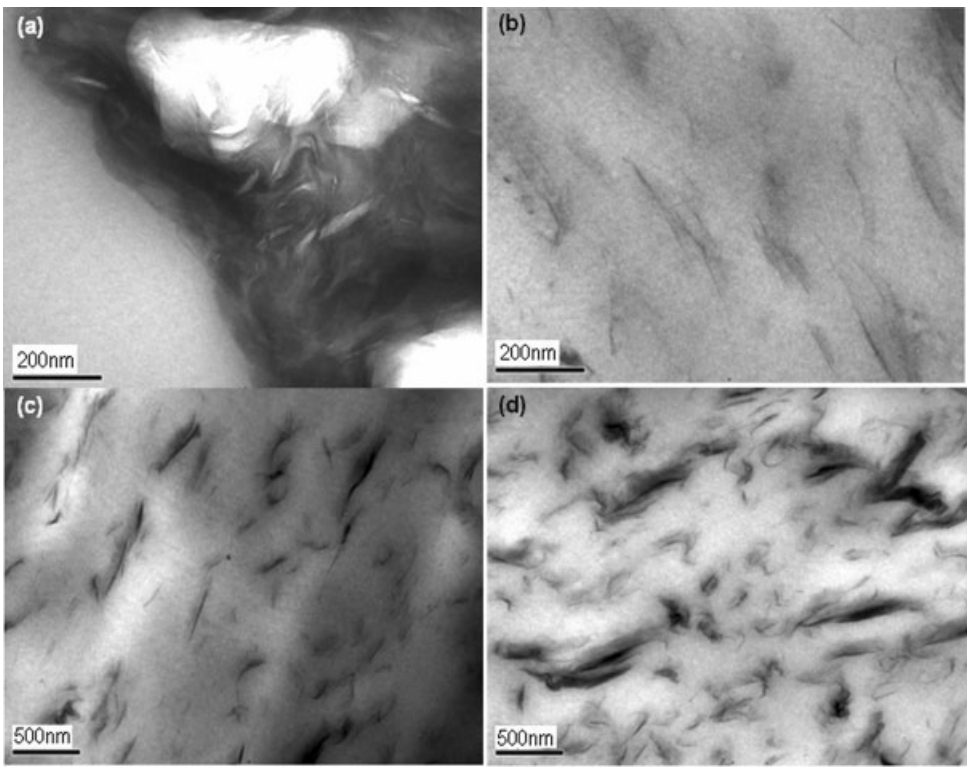

Figure 2 TEM images of (a) 94/0/6, (b) 76/18/6, (c) 88/6/6, and (d) 80/10/10 samples.

clay may attack the partially positive region in the MA ring, causing its rupture and forming a covalent bond with the carbonyl group. The viability of this kind of chemical interaction between clay and PP-*g*-MA is supported by the fact that the OH groups are absent in the dimethyl dehydrogenated tallow quaternary ammonium chloride used for clay modification. The OH side groups of clay are not easily accessible, and this implies that a significant number of MA groups are necessary for the reaction. Proving this reaction mechanism is outside the scope of this work and should be the subject of further research.

Barrier properties

The small size and low interaction capacity of helium molecules with polymer chains make them highly permeable and useful for investigating the structural modifications induced by changes in the formulation of the nanocomposites. Figure 4 shows the helium leak measurements for various systems, which indicate that the addition of clay to the PP matrix without the compatibilizer brings about a reduction in the gas flow. Additional improvements in the helium barrier properties are obtained for higher concentrations of the compatibilizer as the amount of the filler remains constant (6 wt %). This effect can be explained by changes in the arrangement of the clay platelets and by the state of the amorphous domains. The insertion of inorganic particles into the homopolymer matrix, even if they remain in poorly intercalated stacks, is likely to decrease the mobility of the amorphous phase, which in turn is directly related to the gas diffusivity.[18] Amorphous chains located in the vicinity of the rigid particles do not entangle with one another and become locally oriented and strained, thereby hindering the permeation of gas molecules. When the compatibilizer is included in the formulation (6 or 18 wt %), the polymer–clay interactions become stronger, and the stack configuration is modified, as shown by TEM images. The smaller clay aggregates and individual platelets are then dispersed in the matrix, increasing tortuosity, and induce the partial alignment of nearby amorphous chains; these combined actions lead to an overall improvement in the barrier properties. Figure 4 also shows that the performance of the sample with low concentrations of both the filler and compatibilizer (3 wt % each) was comparable to that of the system with no PP-*g*-MA but with a larger content of filler (6 wt %), proving that a certain concentration of particles has the same effect as a moderately smaller concentration mixed with the compatibilizer. Finally, the helium leak detected for the PP matrix containing 10 wt % of both nanoparticles and PP-*g*-MA was remarkably higher than that corresponding to any other formulation, probably because the filler concentration was too high and the available PP-*g*-MA

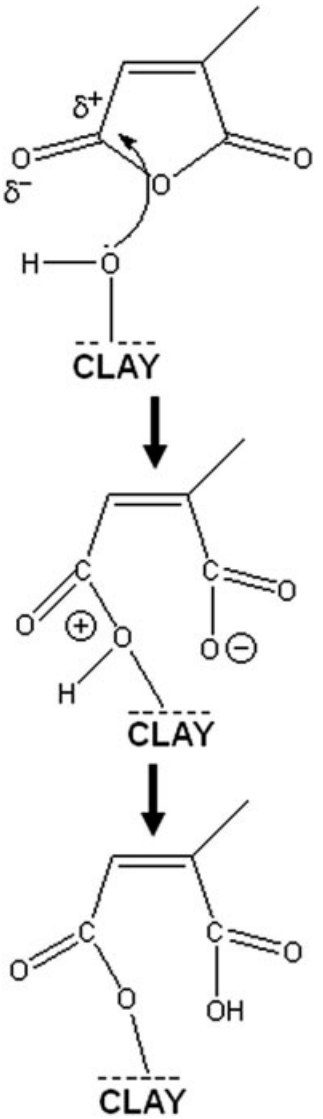

Figure 3 Proposed mechanism for the reaction between clay and MA.

molecules were not enough to compatibilize the system and modify the stack structures. The lack of interactions between PP chains and excess inorganic tactoids might lead to the formation of voids in the structure that boost gas diffusivity.

The results issued from the evaluation of WVTR show that the hydrophobic PP matrix loses its good barrier properties against water when blended with hydrophilic clay particles (Fig. 5). This behavior can be explained by the affinity of the clay surface for water molecules, which can be adsorbed onto these sites and form channels in the polymer matrix between neighboring particles, thus increasing the WVTR of the nanocomposites. A further increase in the concentration of the compatibilizer deteriorates even more the barrier properties of the material. Paradoxically, the higher degree of exfoliation and dispersion of the nanoparticles in the compatibilized system (confirmed by TEM and WAXD) is thought to improve the permeation of water molecules by providing a broader network of sites for channel formation.

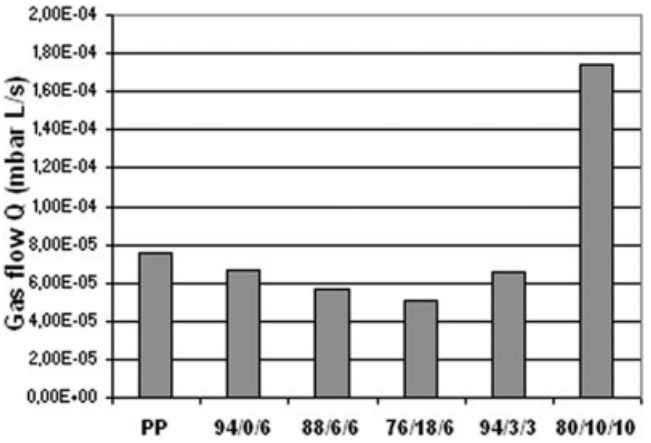

Figure 4 Helium leak measurements for neat PP and PP/PP-*g*-MA/OMMT nanocomposites (performed at 23°C).

The assessment of the barrier properties of PP/PP-*g*-MA/OMMT nanocomposites with respect to organic solvents was performed with methanol and toluene, which differ with respect to the molecular dimensions and the degrees of interaction with the polymer matrix (methanol is a polar solvent, whereas toluene molecules are nonpolar). The values obtained in transmission rate tests are summarized in Figure 6 for methanol and in Figure 7 for toluene. In the case of methanol, Figure 6 reveals that the unmodified PP exhibits better barrier properties than the systems prepared with PP-*g*-MA, OMMT particles, or both. Blending PP with PP-*g*-MA facilitates the transport of methanol molecules, and this implies that the solvent molecules interact with the MA group. An additional slight increase in the transmission rate can be observed for the PP/OMMT system without

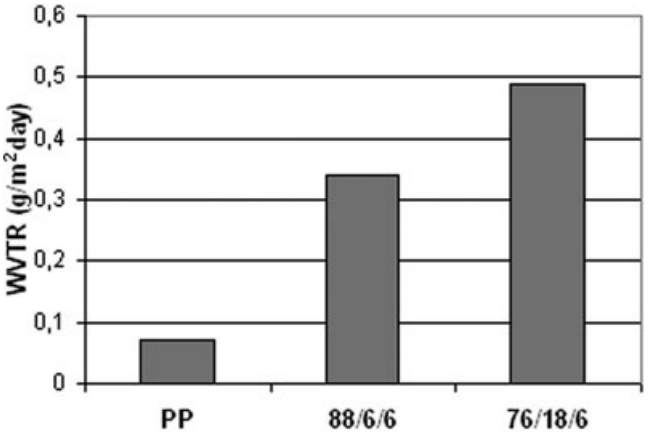

Figure 5 WVTR measurements for neat PP and PP/PP-*g*-MA/OMMT nanocomposites (performed at 23°C).

the compatibilizer, which might be the result of the interactions between the OH groups of methanol and clay. The partially exfoliated structure that develops in the compatibilized 76/18/6 nanocomposite offers better permeation pathways to methanol molecules, and the transmission rate is accordingly enhanced. The PP-*g*-MA molecules are largely responsible for this outcome because of their specific interactions with methanol and their role in the exfoliation and dispersion of silicate layers, making available the OH groups of clay.

A rough comparison of the mass of methanol and toluene that is able to permeate the tested polymeric materials per day per unit of area confirms that toluene molecules flow more easily because of their overall affinity with the polymer matrix. The results presented in Figure 7 suggest that toluene molecules do not interact with the compatibilizer, and thus the solvent transmission rate in neat PP remains practically unchanged when PP-*g*-MA is included in the formulation. However, the barrier properties considerably deteriorate in the presence of OMMT particles. This behavior could result from specific interactions between toluene molecules and the organic surfactant present in clay layers (dimethyl dehydrogenated tallow quaternary ammonium chloride). The magnitude of such interactions can be quantified by the polymer–solvent interaction parameter (χ):[19]

$$\chi = 0.34 + \frac{V_S}{RT}(\delta_P - \delta_S)^2 \quad (1)$$

In this expression, V_S is the molar volume of the solvent (cm^3/mol), δ_P is the solubility parameter of the surfactant, δ_S is the solubility parameter of toluene, R is the gas constant, and T is the experimental temperature (K). The values of the solubility parameter

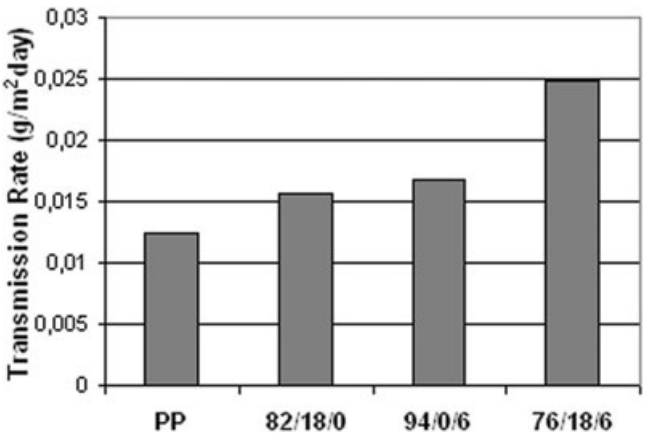

Figure 6 Methanol transmission rate results for neat PP and various PP/PP-*g*-MA/OMMT composites (with a compatibilizer and/or filler nanoparticles). The average testing time was 7 days.

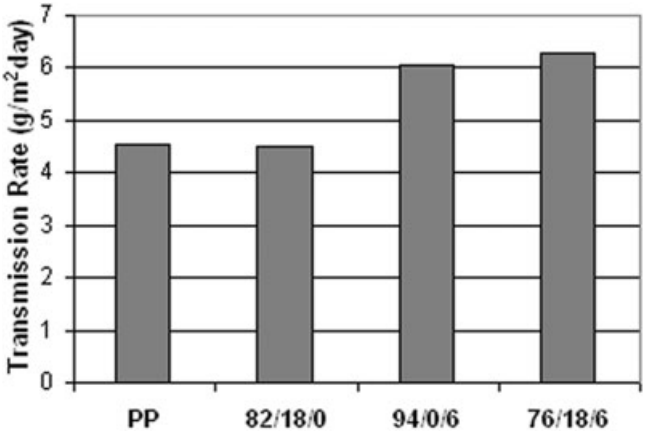

Figure 7 Toluene transmission rate results for neat PP and various PP/PP-*g*-MA/OMMT composites (with a compatibilizer and/or filler nanoparticles). The average testing time was 40 days.

(δ) for each chemical species can be theoretically calculated by the group contribution method:[20]

$$\delta = \frac{\rho \sum G}{M} \quad (2)$$

This method is based on the density (ρ) of the compound, its molecular weight (M), and the summation of the molar attraction constants (G) of all the structural groups that constitute the molecule (values derived from measurements of the heat of evaporation and reported in refs. 19 and 20).

In brief, calculations for δ_P and δ_S yielded the following results: 17.33 and 18.69, respectively. With a value of 104.9 for V_S in eq. (1), χ was 0.41, which indicated thermodynamically favorable interactions between toluene and the quaternary ammonium salt added to natural clay. Such interactions are only physical, and no chemical reaction is implied, as confirmed by IR spectroscopy (the IR spectra were very conventional and are not reported here). The estimation process was repeated for toluene and unmodified clay, providing a high and positive result of $\chi = 164.47$, which suggests rather unfavorable interactions for that particular system. In brief, it can be concluded that the high toluene transmission rate in PP/OMMT nanocomposites is due to the affinity between the solvent molecules and the organic surfactant of the clay. This phenomenon is practically unaffected by the presence of compatibilizer molecules in the system, as shown by Figure 7.

It is clear that the use of MA improves the state of exfoliation and dispersion of OMMT in the PP matrix. However, the presence MA favors the penetration of polar solvents and dramatically degrades the barrier properties of virgin PP. A different type of clay (more inert) would be required to reduce the interactions with the permeant molecules in the nanocomposites.

CONCLUSIONS

This study on the morphology and barrier properties of polymer–clay nanocomposites provides valuable information about the structural features and specific interactions developed by changes in the composition (filler and compatibilizer contents) and their influence on barrier performance. Strong interactions between the filler and the permeant molecules, which are intensified by the state of exfoliation and dispersion of clay the layers induced by the compatibilizer, are critical. Additionally, a mechanism based on the interactions between clay and MA groups of the compatibilizer has been proposed to explain the development of the desirable dispersed nanostructure.

Overall, the unmodified PP exhibits fairly better barrier performance than its mixtures with PP-*g*-MA and/or OMMT; the only improvement has been obtained for the helium barrier properties. This negative effect has been explained by the interactions occurring between the diffusing molecules and the inherently hydrophilic clay or the quaternary ammonium salt used as a surfactant in the organically modified silicate layers.

To improve the barrier properties of the nanocomposites, it would be interesting to explore different approaches, such as the use of a different type of clay (more inert), sample annealing to rearrange and reduce the free volume in the disordered amorphous domains and modify the state of the impermeable crystalline domains, and particle orientation during sample processing.

Thanks are due to Steve Pouliot and Marlaine Rousseau for their valuable collaboration.

References

1. Osborn, K. R.; Jenkins, W. A. Plastic Films: Technology and Packaging Applications; Technomic: Lancaster, PA, 1992.
2. Faisant, J. B.; Aït-Kadi, A.; Bousmina, M.; Deschênes, L. Polymer 1998, 39, 533.
3. Osman, M. A.; Rupp, J. E. P.; Suter, U. W. J Mater Chem 2005, 15, 1298.
4. Yano, K.; Usuki, A.; Okada, A. J Polym Sci Part A: Polym Chem 1997, 35, 2289.
5. Carrado, K. A. In Advanced Polymeric Materials; Shonaike, G. O.; Advani, S. G., Eds.; CRC: Boca Raton, FL, 2003; Chapter 10.
6. Sinha Ray, S.; Okamoto, M. Prog Polym Sci 2003, 28, 1539.
7. Hasegawa, N.; Okamoto, H.; Kato, M.; Usuki, A. J Appl Polym Sci 2000, 78, 1918.
8. Reichert, P.; Nitz, H.; Klinke, S.; Brandsch, R.; Thomann, R.; Mülhaupt, R. Macromol Mater Eng 2000, 275, 8.
9. Nam, P. H.; Maiti, P.; Okamoto, M.; Kotaka, T.; Hasegawa, N.; Usuki, A. Polymer 2001, 42, 9633.
10. Maiti, P.; Nam, P. H.; Okamoto, M.; Hasegawa, N.; Usuki, A. Macromolecules 2002, 35, 2042.
11. Marchant, D.; Krishnamurthy, J. Ind Eng Chem Res 2002, 41, 6402.
12. Lertwimolnum, W.; Vergnes, B. Polymer 2005, 46, 3462.
13. Gorrasi, G.; Tortora, M.; Vittoria, V.; Kaempfer, D.; Mülhaupt, R. Polymer 2003, 44, 3679.
14. Gorrasi, G.; Tammaro, L.; Tortora, M.; Vittoria, V.; Kaempfer, D.; Reichert, P.; Mülhaupt, R. J Polym Sci Part B: Polym Phys 2003, 41, 1798.
15. Alberola, N.; Fugier, M.; Petit, D.; Fillon, B. J Mater Sci 1995, 30, 1187.
16. Shanks, R. A.; Yu, L. In Polymeric Materials Encyclopedia; Salamone, J. C., Ed.; CRC: Boca Raton, FL, 1996; Vol. 8.
17. Guan, Y.; Wang, S.; Zheng, Z.; Xiao, H. J Appl Polym Sci 2003, 88, 872.
18. Polyakova, A.; Liu, R. Y. F.; Schiraldi, D. A.; Hitner, A.; Baer, E. J Polym Sci Part B: Polym Phys 2001, 39, 1889.
19. Mark, J. E. Physical Properties of Polymers Handbook; American Institute of Physics: Woodbury, 1996.
20. van Krevelen, D. W. Properties of Polymers, 3rd ed.; Elsevier: Amsterdam, The Netherlands, 1990.